THE ASTROPHYSICAL JOURNAL, 434:244–261, 1994 October 10

HIGHLY IONIZED GAS IN THE GALACTIC DISK: THE $l = 295°$, $b = 0°$ INTERARM DIRECTION

KENNETH R. SEMBACH[1]
Center for Space Research, 6-216, Massachusetts Institute of Technology, 77 Massachusetts Avenue, Cambridge, MA 02139
(I): sembach@sundoggie.mit.edu
Received 1994 January 24; accepted 1994 April 22

ABSTRACT

I present new high-resolution measurements of ultraviolet interstellar absorption lines toward three distant stars in the Galactic disk in the general direction $l = 295°$, $b = 0°$. The high ionization lines of Si IV and C IV toward HD 100276, HD 103779, and HD 104705 show substantial variations on angular scales of less than 1°, or about 50–100 pc at the distance of the stars. The Si IV and C IV midplane densities derived for HD 100276 and HD 103779 are n_0(Si IV) $\approx 1.3 \times 10^{-9}$ cm^{-3} and n_0(C IV) $\approx 4.5 \times 10^{-9}$ cm^{-3}, approximately a factor of 2–3 lower than the Galactic averages found by Sembach & Savage (1992). Toward HD 104705, the Si IV midplane density is near the average value, but the C IV midplane density is a factor of 3 higher than average. The integrated C IV and Si IV ratios along the HD 100276 and HD 100379 sight lines are similar to the N(C IV)/N(Si IV) $= 3.6 \pm 1.3$ ratio found by Sembach & Savage (1992) for a sample of halo stars. For the HD 104705 sight line, N(C IV)/N(Si IV) = 11 and N(C IV)/N(N V) > 10. Turbulent mixing layers provide a possible source for the observed absorption along the three sight lines as does gas associated with cooling flows. If mixing layers are the primary source of the absorption along the disk sight lines, then the entrainment velocity of the hot gas is $\sim$100 km s^{-1} and the post–mixed gas temperature is $\approx 2 \times 10^5$ K; same differences may exist for these mixing layers compared to those inferred for gas toward the Galactic poles. Current models of cooling, hot gas in supernova remnants, and magnetized conduction fronts do not accurately describe the high ion properties toward the disk stars in this study.

Subject headings: ISM: abundances — stars: individual (HD 100276, HD 103779, HD 104705) — turbulence — ultraviolet: ISM

1. INTRODUCTION

Great strides have been made in understanding the properties of highly ionized gas in the Galaxy over the past several years from both observational and theoretical perspectives. Most of the observational studies have focused upon ultraviolet absorption-line measurements of the interstellar material toward distant O and B stars (Pettini & West 1982; Savage & Massa 1987; Sembach & Savage 1992; Spitzer & Fitzpatrick 1992) or bright QSOs or Seyfert nuclei (Savage et al. 1993a, b; Lu, Savage, & Sembach 1994). These observational studies have provided firm detections of Si IV, C IV, and N V and reveal the general prevalence of hot ($T \sim 10^5$ K) gas extending up to several kiloparsecs from the Galactic plane. Recent detections of these species with the Goddard High Resolution Spectrograph (Savage, Sembach, & Cardelli 1994; Savage & Sembach 1994) indicate that the observed absorption profiles arise from a blend of two different types of highly ionized gas. A canonical N(C IV)/N(Si IV) ratio of 3–3.5 is favored by the cooler dominant phase, whereas the hotter ($T \approx 3$–8×10^5 K) less pronounced phase has little Si IV and N(C IV)/N(N V) ≈ 1. Observational evidence for systematic changes in the physical conditions in halo gas as a function of distance away from the plane is scarce, although measurements of Si IV and C IV for the HD 116852 sight line indicate that the level of ionization may change with $|z|$ (Sembach & Savage 1994).

There are good reasons to suspect that highly ionized disk and halo gas may have different physical properties. Shull & Slavin (1994) favor an inhomogeneous interstellar medium in which superbubbles and turbulent mixing layers account for most of the highly ionized gas at large z-distances and isolated supernova remnants are responsible for the high ionization absorption in the disk. Slavin & Cox (1992, 1993) also note the general problem of producing the high ionization species at large z-distances by isolated supernova bubbles, and for the classical Galactic fountain (Shapiro & Field 1976; Bregman 1980; Edgar & Chevalier 1986; Shapiro & Benjamin 1993), one expects the disk gas to be much hotter ($T \sim 10^6$ K) so that it can rise under its own buoyancy before it cools and recombines to form detectable ultraviolet species.

We have reached a point where we may now know more about highly ionized halo gas than we do about its counterpart in the Galactic disk. Some of the more important questions concerning disk gas that need to be addressed are the following:

1. Do disk and halo gas differ systematically in their physical properties (i.e., temperature, density)?
2. What are the midplane densities of Si IV, C IV, and N V and do they differ along interarm and Galactic center directions?
3. What is the origin of highly ionized disk gas and how does it relate to highly ionized halo gas?
4. Are interarm regions in the disk the "base" of the Galactic halo?

This study is intended to close this information gap and provide a partial understanding of the properties of highly ionized disk gas. In this paper, I present new ultraviolet spectroscopic observations of three stars in the general direction $l = 295°$, $b = 0°$. The stars (HD 100276, HD 103779, and HD 104705) lie within 3° of each other and have distances of 3–5 kpc. I obtained these observations as part of a larger program

[1] Hubble Fellow. Guest Observer with the *International Ultraviolet Explorer* Satellite, sponsored and operated by the National Aeronautics and Space Administration (USA), the Science and Engineering Research Council (UK), and the European Space Agency.

to explore the general properties of the highly ionized interstellar medium in the Galactic disk along extended sight lines using the spectrographs aboard the *IUE* spacecraft. Sections 3 and 4 contain a summary of the observed absorption structure and an overview of the general direction being studied. In § 5 I discuss the analysis techniques used to derive the results presented in § 6. Section 7 contains a discussion of the highly ionized gas in the context of current models of highly ionized gas production. Section 8 addresses circumstellar absorption, and § 9 describes a possible disk-halo connection for the highly ionized gas. A summary of the main conclusions of the paper is located in § 10.

2. *IUE* OBSERVATIONS

I obtained high-dispersion SWP (1150–2000 Å) and LWP (2000–3000 Å) images of HD 100276, HD 103779, and HD 104705 during the summer of 1993 as part of a 16th episode *IUE* program designed to study highly ionized interstellar disk gas. For each star, several exposures were obtained at various locations in the large (10″ × 20″) entrance aperture to sample different portions of the *IUE* Vidicon detector and shift the relative positions of fixed pattern noise structures in the echellograms. At least one new image of each star was acquired with the starlight centered in the large aperture to provide a velocity template for the offset images. Spectral extraction, calibration, order overlap and background corrections, and spectrum merging procedures were identical to those outlined by Sembach & Savage (1992). Table 1 contains a log of the observations obtained for this study. Column (5) of that table contains the velocity shifts required to bring the spectra for each object into a common heliocentric velocity frame. The corrections required to convert the heliocentric velocities into LSR velocities are located in Table 2 (see Mihalas & Binney 1981). The combined spectra have velocity resolutions of 20–25 km s^{-1} (FWHM) and S/N ≈ 10–25.

3. ABSORPTION-LINE SUMMARY

Figures 1–3 contain absorption line profiles for selected low- and high-ionization species detected toward HD 100276, HD 103779, and HD 104705. Many of the absorption lines shown in these figures are blends of stellar and interstellar features. Dashed lines indicate the stellar continua adopted for those lines where the interstellar and stellar contributions can be distinguished from one another. The Si III* λ1294 line illustrated in the right-hand panel of each figure arises out of an excited level of Si III in the stellar photosphere and provides an estimate of the stellar profile. For HD 104705, the stellar profile is broadened substantially by the large rotational velocity of the star ($v \sin i = 217$ km s^{-1}), and most of the interstellar lines are clearly defined. For HD 100276 and HD

TABLE 1

IUE HIGH-DISPERSION ECHELLE SPECTRA

Image (1)	Day/Year (2)	Exposure (minutes) (3)	Aperture Position (4)	Shift (km s^{-1}) (5)	Comment (6)
			HD 100276		
SWP 22147.....	030/1984	42	Center	+16	Archival image
SWP 48190.....	202/1993	35	Center	0	Default velocity template
SWP 48191.....	202/1993	40	−5′ Offset	+26	
SWP 48192.....	202/1993	47	+5′ Offset	−30	
SWP 48193.....	202/1993	45	−5′ Offset	+30	
LWP 25956.....	202/1993	22	Center	0	Default velocity temperature
LWP 25957.....	202/1993	22	−5′ Offset	−25	
LWP 25958.....	202/1993	22	+5′ Offset	+24	
			HD 103779		
SWP 22146.....	030/1984	35	Center	+17	Archival image
SWP 48233.....	206/1993	42	Center	0	Default velocity template
SWP 48234.....	206/1993	30	+5′ Offset	−27	
SWP 48235.....	206/1993	45	−5′ Offset	+24	
SWP 48236.....	206/1993	35	+5′ Offset	−27	
SWP 48237.....	206/1993	55	Center?	−18	Centering uncertain
LWP 25996.....	206/1993	18	+5′ Offset	+27	
LWP 25997.....	206/1993	20	Center	0	Default velocity template
LWP 25998.....	206/1993	17	−5′ Offset	−24	
			HD 104705		
SWP 22418.....	030/1984	60	Center	+10	Archival image
SWP 48194.....	202/1993	45	Center	0	Default velocity template
SWP 48212.....	204/1993	55	−5′ Offset	+16	
SWP 48213.....	204/1993	50	+5′ Offset	−42	
SWP 48214.....	204/1993	55	−5′ Offset	+15	
LWP 25959.....	202/1993	30	Center	0	Default velocity template
LWP 25973.....	204/1993	30	−5′ Offset	−19	
LWP 25974.....	204/1993	30	+5′ Offset	+25	
LWP 25975.....	204/1993	25	−5′ Offset	−20	

TABLE 2

SIGHT LINE INFORMATION[a]

SIGHT LINE	MK	V (mag)	$E(B-V)$ (mag)	l	b	d (kpc)	z (kpc)	$v \sin i$ (km s^{-1})	v_{rad} (km s^{-1})	$v_r(d)$ (km s^{-1})	Δv_{LSR} (km s^{-1})	log N H I	log N Na I	log N Ca II
HD 100276.....	B0.5 Ib	7.16	0.26	293°.31	+0°.77	3.0	+0.04	121	−16	−23	−7.3	21.19	13.31	12.89
HD 103779.....	B0.5 Iab	7.20	0.21	296.85	−1.02	4.1	−0.07	148	−10	−31	−6.7	21.16	13.06	12.79
HD 104705.....	B0 Ib	7.76	0.26	297.45	−0.34	3.9	−0.02	217	−23	−32	−6.5	21.11	12.98	12.81
HD 116852.....	O9 III	8.47	0.22	304.88	−16.13	4.8	−1.32	115	−47	−46	−6.4	20.96	12.82	12.85

[a] See Sembach, Danks, & Savage 1993 for original references.

103779, the stellar profiles are narrower ($v \sin i < 150$ km s^{-1}) and less easily separated from some of the interstellar lines.

Blending is least problematic for the high-ionization lines toward these stars since the Si IV and C IV lines lie on relatively well-developed P Cygni profiles, although the N V P Cygni profiles are less pronounced and stellar blending prevents meaningful estimates of the interstellar N V absorption toward HD 100276 and HD 103779. Figure 4 shows a comparison of the 1240 Å and 1550 Å spectral regions of HD 104705 with those of the B0 Ib standard star 69 Cygni ($v \sin i \approx 90$ km s^{-1}). For the N V lines, the standard star shows similar broad structure, suggesting that much of the absorption at these wavelengths is stellar in nature. However, the upper limit derived using the illustrated continuum (see § 5) places a useful constraint on the amount of hot gas along the sight line (see § 7). For comparison, note the nearby interstellar Mg II lines, which are considerably narrower in both spectra. No photospheric contamination is present for the C IV lines. The small amount of C IV present in the 69 Cygni spectrum is due to interstellar absorption along the 2 kpc line of sight.

The most noteworthy aspect of the ionized species absorption profiles shown in Figures 1–3 is the very strong C IV absorption between 0 and −100 km s^{-1} toward HD 104705. The absorption is much stronger than that seen toward the other stars even though they are less than a few degrees apart. It is also much stronger than the Al III and Si IV absorption at these velocities. A predominantly interstellar origin for the absorption seems certain given that it is seen in spectra taken 9.5 yr apart (see Table 1). Narrow absorption-line components (NACs) are usually present in the winds of early-type stars at very large velocities, $v \approx v_\infty$, and are short lived with changes occurring on timescales of hours or days (Snow 1977; Prinja & Howarth 1986; Prinja, Howarth, & Heinrichs 1987; Howarth et al. 1993). Continuum distortions and photospheric absorptions related to NACs in early stages of development are much broader than the observed features and cannot account for the narrow C IV structure. I discuss possible interstellar and circumstellar origins for the C IV absorption in §§ 7 and 8.

Sembach, Danks, & Savage (1993) have presented high-resolution measurements of the interstellar Na I D and Ca II K lines toward the stars observed in this study. The Na I and Ca II spectra illustrated in the top panels of Figures 1–3 have S/N ≈ 100–200 and resolutions of 4.4 km s^{-1} (FWHM). The spectra reveal a complex system of at least five to six absorption lines in this general direction. The strong, low-ionization lines of C II, Si II, and Fe II trace lower column density gas than the optical lines and span velocity ranges comparable to those spanned by the high-ionization lines. The presence of low ion gas at velocities where the high ion lines are detected is important for understanding the processes that give rise to the higher ionization states (see § 7).

4. DIRECTION OVERVIEW

The general properties of the HD 100276, HD 103779, and HD 104705 sight lines are contained in Table 2.[2] The stars lie within the disk of the Galaxy (i.e., $|z| < 70$ pc in the general direction $l = 295°$, $b = 0°$. Of the three stars, HD 100276 is the closest at 3 kpc and HD 103779 and HD 104705 have distances of approximately 4 kpc. The maximum angular separation of the three stars is 2°.8, corresponding to an angular size of 146 pc at $d = 3$ kpc. HD 104705 and HD 103779 are closer together and have an angular separation of only 0°.8, or 56 pc at $d = 4$ kpc. These sight lines sample mainly low-density disk gas in the form of intercloud and diffuse cloud material; it is unlikely that any large cold clouds are sampled given that the total color excesses are less than those for individual cold clouds (Sembach & Danks 1994).

The spectroscopic distances for the stars listed in Table 2 result from the absolute magnitude–MK spectral type calibration given by Walborn (1972), the intrinsic stellar colors given by Johnson (1963), and $A_V = 3.1\ E(B-V)$. The ultraviolet properties of these stars, particularly HD 100276, were explored by Savage & Massa (1987), who concluded that the ultraviolet spectra are consistent with the listed MK spectral types. The radial velocities of the stars are also comparable to those expected for stars at these distances [compare v_{rad} with $v_r(d)$ in Table 2]. The errors on the calculated distances are probably less than 25%, or about 1 kpc.

The H I column densities inferred from Lyα absorption (Diplas & Savage 1994) for HD 100276, HD 103779, and HD 104705 are within 20% of each other (see Table 2) and indicate that most of the neutral gas seen in absorption in front of the stars is common to all three sight lines. The nearby, low-latitude HD 116852 halo sight line ($l = 305°$, $b = -16°$, $d = 4.8$ kpc, $z = -1.3$ kpc) also has a comparable amount of H I 21 cm emission. The H I 21 cm emission maps presented by Kerr et al. (1986) in this direction show that the detailed character of the H I along these sight lines changes but that the overall velocity structure is preserved. Positive velocities do not result for gas participating in Galactic rotation until line of sight distances of 7 kpc are reached, and therefore some of the higher positive velocity H I gas must occur either at peculiar velocities with respect to the surrounding medium or at large distances. Since much of the 21 cm emission at positive velocities on these maps has no counterpart in the Na I and Ca II lines shown in Figures 1–3, it seems reasonable to conclude that the +50 km s^{-1} and +90 s^{-1} emission complexes in the 21 cm maps must lie well beyond the stars.

[2] I also consider the low-latitude halo sight line toward HD 116852 (see Table 2) in discussions of the disk sight lines in this paper. The reader may find more information about the HD 116852 sight line in the GHRS study presented by Sembach & Savage (1994).

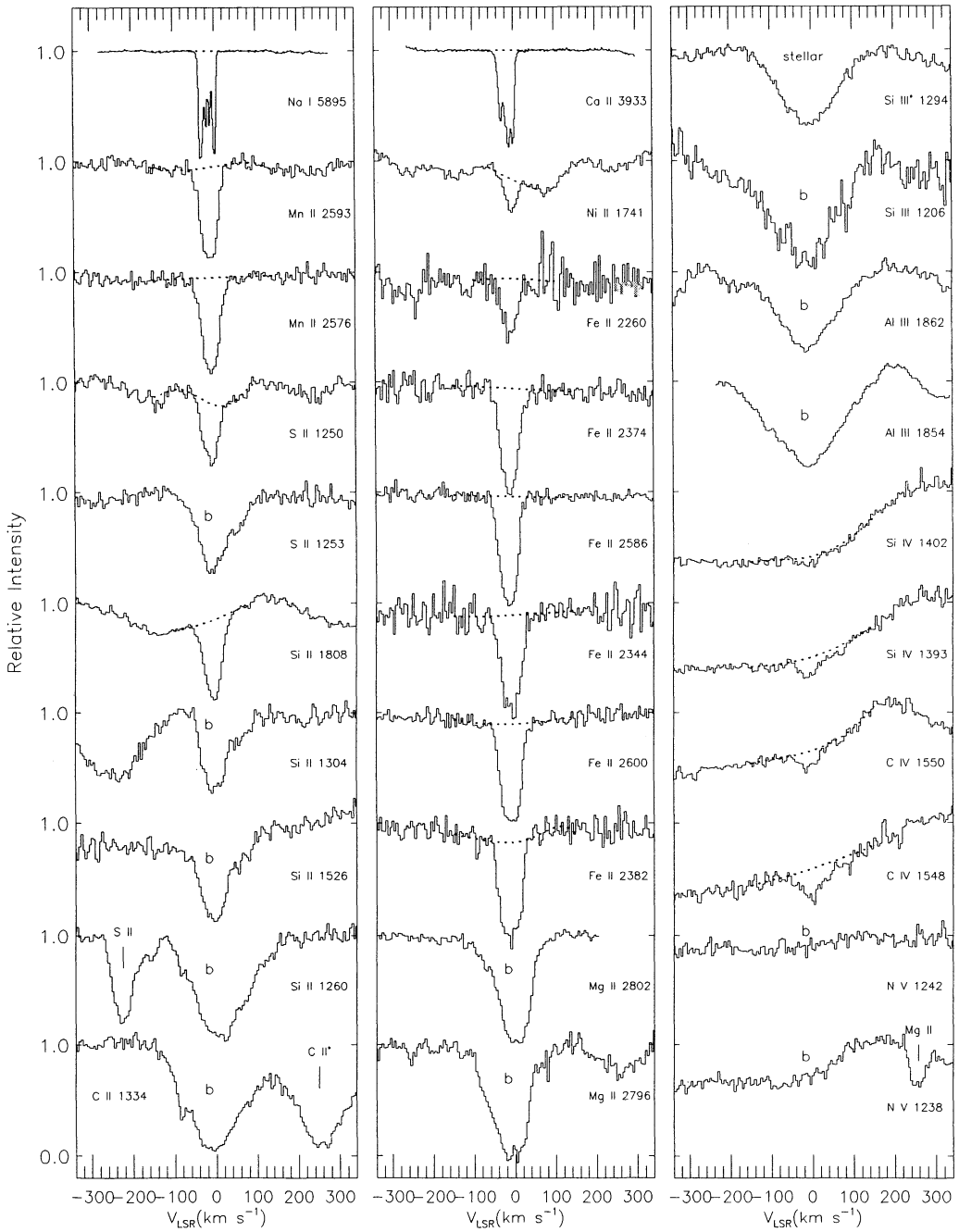

FIG. 1.—Relative intensity vs. LSR velocity of selected interstellar lines in the spectrum of HD 100276. The composite spectra shown are averages of five to six SWP or three to four LWP spectra obtained at various locations in the large entrance aperture. The data have S/N ≈ 15 to 25 and velocity resolutions of approximately 20–25 km^{-1} (FWHM). The Si III* absorption line shown at the top of the right panel arises from an excited state of Si III in the stellar photosphere and provides a measure of the stellar profile. Dashed lines indicate the continua adopted for the interstellar lines. A "b" indicates that stellar blending is too severe to warrant a continuum estimation. The Na I D1 and Ca II K spectra shown are from Sembach, Danks, & Savage (1993) and have S/N ≈ 100 to 200 and resolutions of 4.4 km s^{-1} (FWHM). Note the rich component structure visible in the high-resolution optical data that is partially visible in the low-ionization lines observed by *IUE*.

The most significant large-scale feature present in this direction is the Sagittarius spiral arm. The arm is located at about 1.5 to 2.0 kpc (Courtès et al. 1970; Bok 1971) and is clearly visible at velocities of −20 to −40 km s^{-1} in the H I 21 cm emission maps presented by Kerr et al. (1986). The sight lines span the interarm regions in front of and beyond the Sagittarius arm, and in the latter case, it is possible that some of the observed absorption is associated with spiral arm gas. Rickard (1974) found peculiar Ca II velocities as large as 40 km s^{-1} in some parts of the Sagittarius arm, but the sight lines studied here do not exhibit much Ca II absorption outside the 0 to −30 km s^{-1} velocity range expected for gas participating in Galactic rotation. Sembach & Danks (1994) find that this interarm direction may be more quiescent than most directions in the

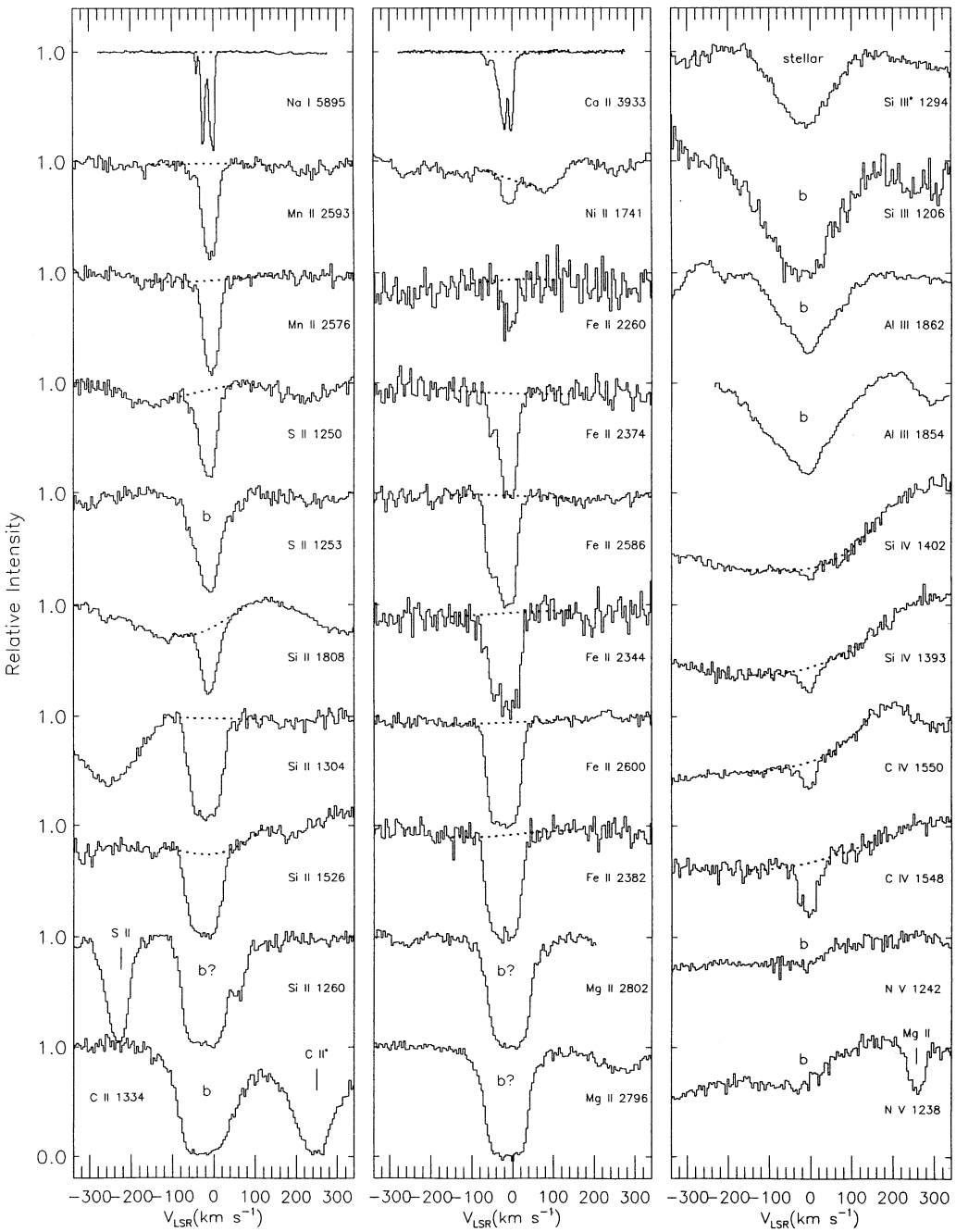

FIG. 2.—Same as Fig. 1, except for HD 103779

Galactic disk (see their Table 4). There is no convincing evidence for absorption associated with the H I and *IRAS* "Galactic worm" emission features seen by Koo, Heiles, & Reach (1992) in this general direction. Of the five Galactic worm candidates with 5° of $l = 295°$, only one (GW 297.8+2.6) lies within 3° of the Galactic plane, and both the distance and H I column density are very uncertain [$d = 3.8$? kpc, N(H I) = $(3.2 \pm 3.8) \times 10^{20}$ cm^{-2}]. The velocities of the Na I and Ca II components shown in Figures 1–3 correlate much better with smaller scale H I 21 cm structures than with other emission features.

The $l = 295°$, $b = 0°$ direction lies near the edge of the *M*-band X-ray enhancement attributed to the North Polar spur (NPS) and Radio Loop I. The all-sky *M*-band X-ray maps presented by McCammon et al. (1983) have point sources removed in this direction, but the outline of Loop I is visible nearby. H I 21 cm maps of Loop I at latitudes greater than 10° show small-scale structure in the $l = 295°$ direction at boundaries of the Loops (Heiles 1982). Unfortunately, in the plane of the Galaxy, H I maps of the region are confused by general disk gas in this direction (see the H I plots produced by Kerr et al. 1986). Some of the high-ionization absorption seen along these sight lines could arise in gas associated with the X-ray emission since the total neutral hydrogen columns are comparable to the N(H I) $\sim 10^{21}$ cm^{-2} column required to reach an absorption optical depth of unity in the *M*-band. Sembach & Savage

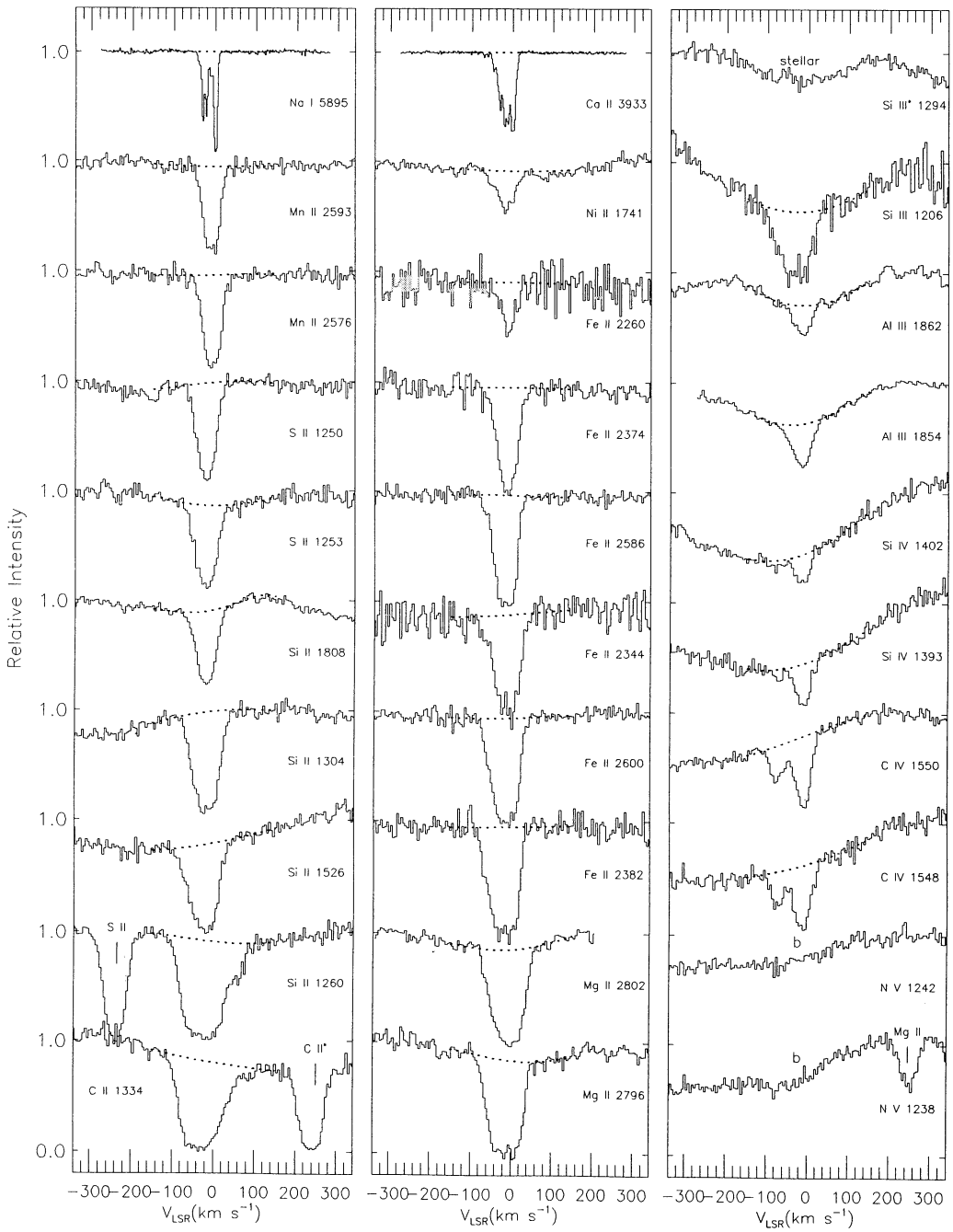

FIG. 3.—Same as Fig. 1, except for HD 104705

(1994; see also Sembach & Savage 1992) find strong Si IV, C IV, and N V, absorption toward HD 116852 that may be related to some of the absorption seen toward HD 100276, HD 103779, and HD 104705. As we shall see in § 6, comparisons of the high-ionization absorption lines in Figures 1–3 with those toward HD 116852 reveal that some of the gas probably has a common origin in the Galactic disk.

5. DATA ANALYSIS

5.1. *Equivalent Widths*

To define the continua for the interstellar lines shown in Figures 1–3, I fitted a low-order (<5) polynomial to regions selected within 300 km s^{-1} of either side of each line. The wavelengths, oscillator strengths, equivalent widths and $\pm 1\ \sigma$ errors, and velocity integration ranges for the lines shown in Figures 1–3 are listed in Table 3. The equivalent width errors reflect uncertainties due to continuum placement uncertainties and statistical noise fluctuations within the lines. The measurement and error propagation methods are identical to those described by Sembach & Savage (1992). For many lines, no measurement was possible with the HD 100276 and HD 103779 data because of stellar blending with the interstellar absorption.

5.2. *Apparent Column Density Profiles and Column Densities*

The equivalent widths listed in Table 3 indicate that saturation effects are important for many of the observed lines due to

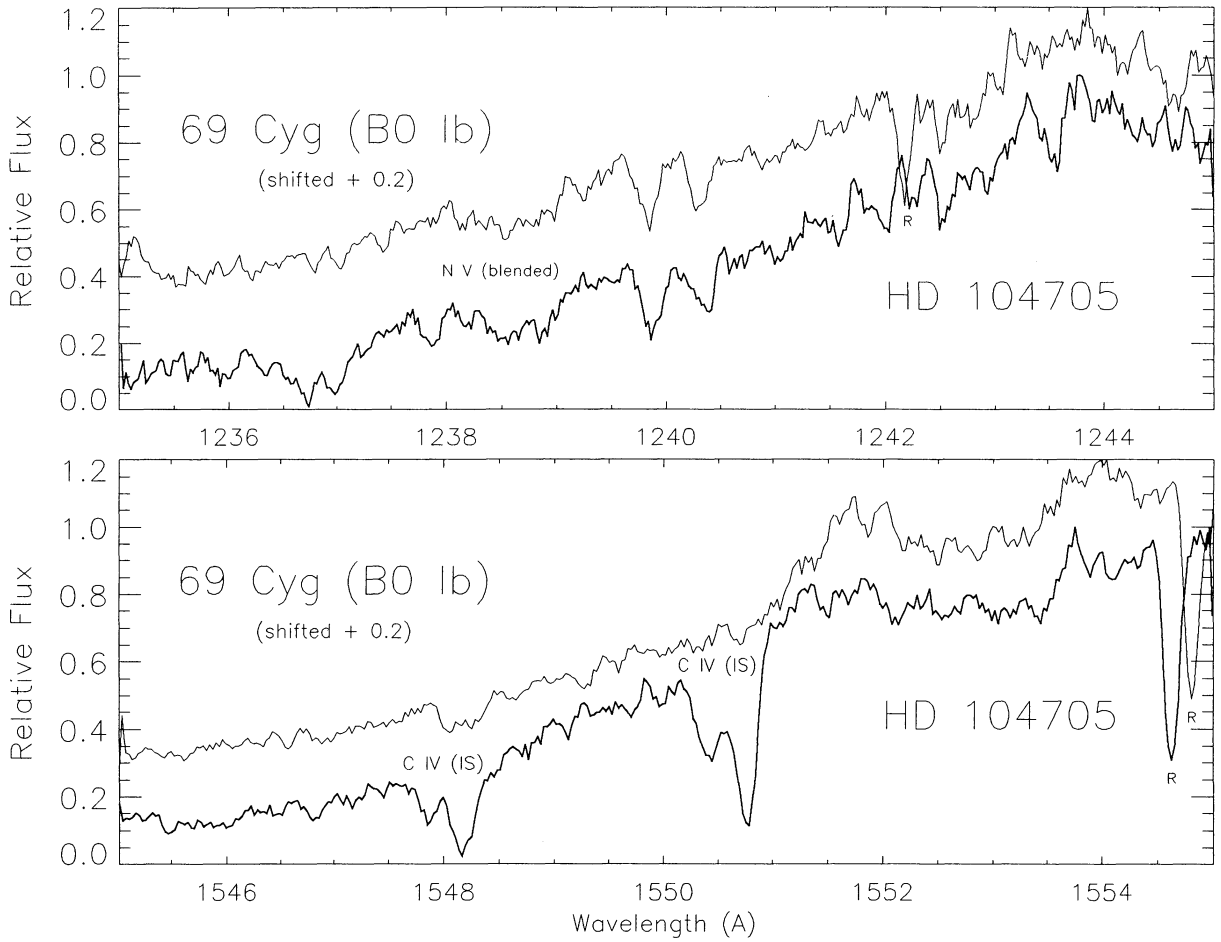

FIG. 4.—Comparison of the relative flux in the 1240 Å and 1550 Å spectral regions of HD 104705 and 69 Cygni (HD 204172), a B0 Ib standard star. The data for 69 Cygni are shifted by +0.2 to facilitate the comparison. For both stars, single well-exposed SWP spectra smoothed with a 5 pixel boxcar filter were used to produce the illustrated spectra. The broad absorption at 1238 Å is characteristic of stars of this spectral type, and it is clear that the interstellar N v absorption is hidden within this absorption. The C IV profiles are free of photospheric contamination; the small amount of C IV absorption seen toward 69 Cygni is interstellar.

the finite instrumental resolution available with *IUE*. These effects are most severe for the strong neutral ion lines and are least important for ionized species like Al III, Si IV, and C IV. To study the absorption in terms of a physically meaningful quantity, it is advantageous to convert the ionized gas lines into measures of apparent column density per unit velocity, $N_a(v)$ [atoms cm^{-2} $(km\ s^{-1})^{-1}$], through the following relation:

$$N_a(v) = \frac{m_e c/\pi e^2}{f\lambda}\,\tau_a(v) = \frac{3.768 \times 10^{14}}{f\lambda}\,\ln\frac{I_c(v)}{I(v)},$$

where $I(v)$ and $I_c(v)$ are the intensities of the line and the estimated continuum at velocity v, $\tau_a(v)$ is the *apparent* optical depth of the line at v, f is the oscillator strength of the transition, and λ is the wavelength of the line in Å. $N_a(v)$ in the above equation is an *apparent* column density per unit velocity because the original absorption line is viewed through an instrumental spread function having a finite resolution. Through numerical simulations Savage & Sembach (1991) have shown that if the $N_a(v)$ profiles for doublet lines agree to within approximately 20%, they provide column density estimates with errors less than this amount, and the individual $N_a(v)$ profiles provide a reliable representation of the true column density per unit velocity convolved with the instrumental spread function. This technique has been successfully exploited by Sembach & Savage (1992) to study the high-ionization profiles constructed from *IUE* data similar to that presented here.

Apparent column density profiles for the interstellar Si IV and C IV lines toward HD 100276 and HD 103779 are shown in Figure 5. Solid and dashed lines indicate the $N_a(v)$ values for the weak and strong line members of each doublet. The error bars for the weak and strong line values are located at the top and bottom of each panel, respectively. For both sight lines, the $N_a(v)$ values within each doublet agree well with one another, indicating that there is little unresolved saturated structure within the profiles.

Apparent column density profiles for the interstellar Al III, Si IV, and C IV lines toward HD 104705 are shown in Figure 6. For Al III and Si IV, the weak and strong line members of each doublet agree well and indicate that the observed values of $N_a(v)$ represent valid instrumentally smeared versions of the true column density profiles. For C IV, the strong line values substantially underestimate the weak line values, indicating that both $N_a(v)$ profiles are affected by unresolved structures and underestimate the true column density profile over much of the velocity range from -100 to $+20$ km s^{-1}.

TABLE 3

EQUIVALENT WIDTHS OF LINES IN ILLUSTRATED FIGURES 1–3[a,b,c]

Ion	λ_{vac} (Å)	f	HD 100276 W_λ (mÅ)	HD 103779 W_λ (mÅ)	HD 104705 W_λ (mÅ)	Range (km s^{-1})
C II	1334.532	1.278 (−1)	...	...	513.1 ± 9.0	−110 to +80
C II*	1335.704	1.149 (−1)	...	...	304.4 ± 16.0	−110 to +80
C IV	1548.195	1.908 (−1)	148.5 ± 18.0	176.4 ± 15.1	324.7 ± 20.0	−130 to +60
C IV	1550.770	9.522 (−1)	62.7 ± 16.3	89.3 ± 11.9	282.5 ± 13.2	−130 to +60
N V	1238.821	1.570 (−1)	...	...	<81.2	−130 to +60
N V	1242.804	7.823 (−2)	...	...	...	...
Mg II	1239.925	2.675 (−4)	55.9 ± 6.6	77.7 ± 11.6	81.3 ± 12.3	−85 to +35
Mg II	1240.395	1.337 (−4)	31.1 ± 11.2	44.5 ± 7.5	60.0 ± 10.5	−85 to ±35
Mg II	2796.352	6.123 (−1)	...	...	889.6 ± 23.9	−110 to +80
Mg II	2803.571	3.054 (−1)	...	...	851.9 ± 15.4	−110 to +80
Al III	1854.716	5.602 (−1)	...	...	206.3 ± 13.5	−130 to +60
Al III	1862.790	2.789 (−1)	...	...	104.2 ± 14.0	−130 to +60
Si II	1260.422	1.007 (0)	...	...	511.8 ± 7.8[d]	−110 to +80
Si II	1304.370	1.473 (−1)	...	348.7 ± 8.9	303.0 ± 8.5	−110 to +80
Si II	1526.707	2.303 (−1)	...	439.0 ± 14.0	401.4 ± 14.3	−110 to +80
Si II	1808.013	5.527 (−3)	246.4 ± 6.4	203.1 ± 7.7	247.2 ± 13.1	−110 to +80
Si III	1206.500	1.669 (0)	...	...	371.8 ± 24.4	−130 to +60
Si IV	1393.755	5.104 (−1)	108.2 ± 19.3	95.7 ± 17.2	184.9 ± 27.5	−130 to +60
Si IV	1402.770	2.553 (−1)	45.1 ± 19.0	37.5 ± 20.8	132.8 ± 24.5	−130 to +60
S II	1250.584	5.453 (−3)	118.1 ± 13.8	174.0 ± 12.4	200.5 ± 8.4	−110 to +80
S II	1253.811	1.088 (−2)	...	...	221.2 ± 11.1	−110 to +80
S II	1259.519	1.624 (−2)	...	...	263.4 ± 10.4	−110 to +80
Mn II	1197.184	1.566 (−1)	...	...	56.5 ± 16.9	−110 to +80
Mn II	2576.877	3.508 (−1)	398.4 ± 17.2	345.0 ± 12.6	396.9 ± 25.6	−110 to +80
Mn II	2594.499	2.710 (−1)	351.8 ± 20.3	330.7 ± 11.2	335.9 ± 17.0	−110 to +80
Mn II	2606.462	1.927 (−1)	316.5 ± 17.6	314.1 ± 17.8	366.5 ± 23.3	−110 to +80
Fe II	2260.780	3.715 (−3)	201.1 ± 60.8	165.4 ± 47.9	160.7 ± 62.2	−110 to +80
Fe II	2344.214	1.097 (−1)	439.9 ± 35.6	603.2 ± 26.3	577.5 ± 52.4	−110 to +80
Fe II	2374.461	3.985 (−2)	400.6 ± 25.8	462.8 ± 30.6	457.9 ± 25.3	−110 to +80
Fe II	2382.765	3.006 (−1)	473.1 ± 35.7	717.2 ± 22.6	646.5 ± 26.6	−110 to +80
Fe II	2586.650	6.457 (−2)	447.7 ± 13.4	615.1 ± 15.2	579.3 ± 18.5	−110 to +80
Fe II	2600.173	2.239 (−1)	494.4 ± 23.1	758.6 ± 11.8	673.0 ± 17.5	−110 to +80

[a] Equivalent widths calculated using the continua shown as dashed lines in Figs. 1–3. All errors are 1 σ errors resulting from continuum placement uncertainties and statistical noise fluctuations in the lines. A 2% background error (not listed) translates into 2% of the listed equivalent widths.

[b] Wavelengths and f-values are from Morton 1991.

[c] A three-dot ellipsis indicates that the line is blended with stellar absorption, and a meaningful interstellar estimate is not possible.

[d] Fe II λ1260.533 present in profile at positive velocities.

The total column density of an ion can be recaptured from apparent column density profiles like those shown in Figures 5 and 6 when there is no unresolved saturated structure by integrating over the velocity range of the absorption [i.e., $N \approx \int N_a(v)dv$]. When saturated structure exists, integrating the $N_a(v)$ profile underestimates the column density and a correction like the one outlined by Savage & Sembach (1991) for doublet lines must be applied. The velocity structure present in the HD 104705 C IV profiles shown in Figure 5 provides a convenient reference for judging the column densities of the ionized species over different velocity ranges. Table 4 contains the apparent column densities for the Al III, Si IV, C IV, and N V lines toward HD 116852 and the three stars in this study for the velocity ranges extending from −130 to −50 km s^{-1}, −50 to +60 km s^{-1}, and +60 to +110 km s^{-1}. The +60 to +110 km s^{-1} interval extends beyond most of the high ion absorption but is included for completeness since there appears to be some Si IV and C IV absorption in this velocity interval toward HD 100276. The ±1 σ errors listed in Table 4 represent contributions from continuum placement uncertainties and statistical noise fluctuations in the lines. A 2% background error contributes approximately 0.01 dex error to the listed values.

Table 5 contains final column densities based upon the apparent column densities listed in Table 4. One sigma limits are transferred from Table 4 and converted to 2 σ limits. When the weak- and strong-line log N_a values within a doublet overlap or when the strong-line value exceeds the weak-line value, the final result is an average of the two estimates. When the weak-line value significantly exceeds the strong-line values, the doublet correction outlined by Savage & Sembach (1991) has been applied to the weak-line values. These column density estimates are statistically identical to those obtained from a single-component Doppler-broadened curve-of-growth analysis using the equivalent widths and errors derived over the same velocity intervals. For sight lines where similar methods have been used (i.e., Sembach & Savage 1992), higher

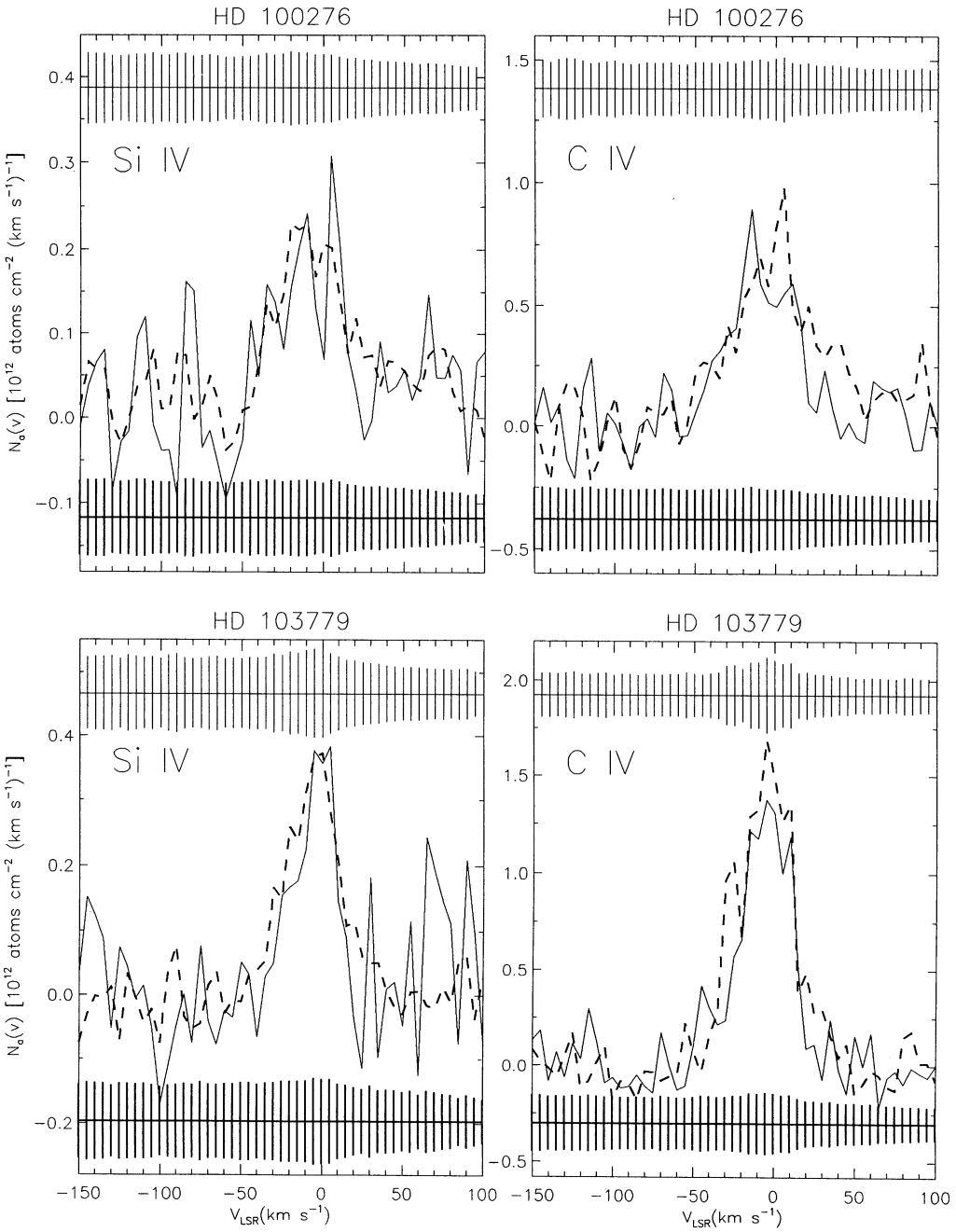

FIG. 5.—Apparent column density profiles, $N_a(v)$ [atoms cm^{-2} (km s^{-1})$^{-1}$], as a function of LSR velocity for the Si IV and C IV lines toward HD 100276 and HD 103779. $N_a(v)$ is defined in the text. The solid and dashed lines indicate $N_a(v)$ for the weak and strong line members of the doublet, respectively. Errors due to continuum placement uncertainties and statistical noise fluctuations in the data are shown at the top of each panel for the weak line and at the bottom for the strong line. Note the good agreement of the $N_a(v)$ profiles within each doublet, indicating that there is little unresolved saturated structure present within the lines.

resolution observations with the Goddard High Resolution Spectrograph aboard the *Hubble Space Telescope* have confirmed that the column densities produced by this method are reliable (see Savage et al. 1994; Sembach & Savage 1994).

Limits on the amount of N V present in each of the three velocity intervals are also given in Table 5 for HD 104705. These limits were determined by integrating the apparent column density profile that results from fitting a third-order polynomial to either side of the absorption near 1238 Å in Figure 3. The continuum is shown in Figure 4 and represents an upper limit to the amount of interstellar N V absorption along the HD 104705 sight line because of contamination with stellar absorption (see § 3).

6. OBSERVATIONAL RESULTS

6.1. *Sight Line Comparisons*

There are clear differences in the amount and velocity structure of the highly ionized gas along the three disk sight lines in this study. The most pronounced difference occurs for C IV,

which is nearly 8 times more abundant along the HD 104705 sight line than along the HD 100276 and HD 103779 sight lines. The HD 104705 sight line also contains 2–3 times more Si IV per unit distance than the HD 100276 and HD 103779 sight lines. These observations show that very large variations in the character of the highly ionized gas absorption occur over size scales as small as 50–100 pc.

Figure 7 contains comparisons of the Al III, Si IV, and C IV profiles for the HD 100276, HD 103779, HD 104705, and HD 116852 sight lines. The positive velocity portions of the HD 100276, HD 103779, and HD 116852 Si IV and C IV profiles agree reasonably well, with differences in the strength of the absorption occurring as a result of the differences in the distances of the three stars. The HD 104705 sight line has much more pronounced Si IV and C IV at low velocities compared to the other sight lines and has additional absorption beyond -50 km s^{-1} that is not visible in the HD 100276 and HD 103779 data.

The Si IV and C IV absorption toward HD 116852 is broader than, and offset from, the main Si IV and C IV absorption toward the disk stars. This is partially the result of differential Galactic rotation effects operating on gas at line-of-sight distances greater than 3 kpc (i.e., $|z| > 800$ pc), and the strength of the high ion absorption toward HD 116852 at velocities beyond -30 km s^{-1} attests to the prevalence of highly ionized gas in the low Galactic halo in this interarm direction. The HD 116852 Si IV and C IV data show no counterpart to the HD 104705 -75 km s^{-1} absorption complex, which further suggests that the HD 104705 high ion absorption is confined primarily to the Galactic disk whereas much of the HD 116852 high ion absorption may arise in the low halo.

The differences in the Si IV and C IV profiles toward HD 104705 and HD 116852 stand in stark contrast to the relative similarity of the Al III profiles along the sight lines (Fig. 7, *top panel*). Both sight lines show Al III absorption over very similar velocity ranges with similar absorption structure. The enhancement of Al III toward HD 116852 over that seen toward HD 104705 compared to the opposite trend in Si IV and C IV suggests that the Al III and higher ions do not trace each other well, either as the result of the gas being more highly ionized in the Galactic disk in this general direction or as the

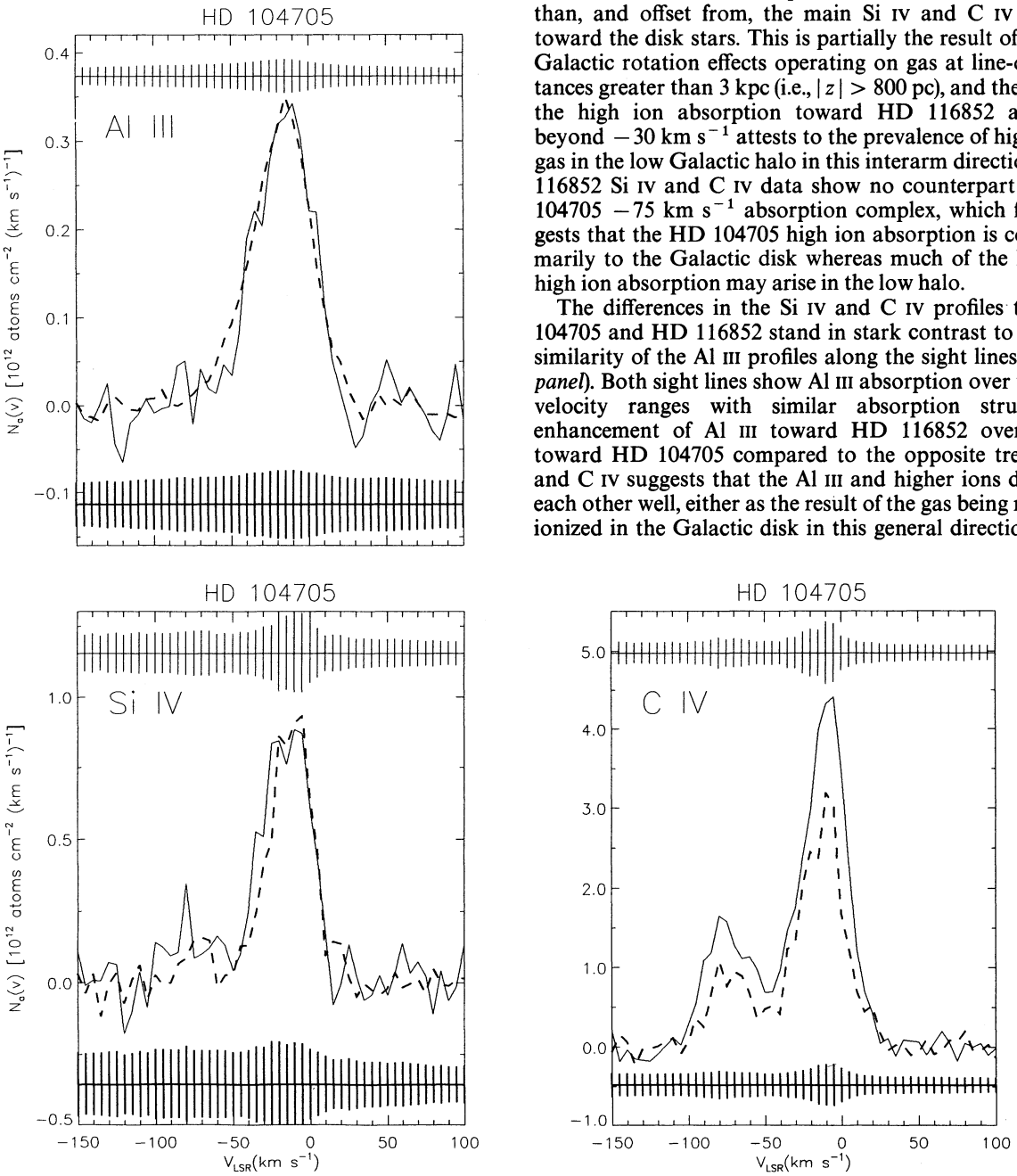

FIG. 6.—Apparent column density profiles, $N_a(v)$ [atoms cm^{-2} (km s^{-1})], as a function of LSR velocity for the Al III, Si IV, and C IV lines toward HD 104705. $N_a(v)$ is defined in the text. The solid and dashed lines indicate $N_a(v)$ for the weak and strong line members of the doublet, respectively. Errors due to continuum placement uncertainties and statistical noise fluctuations in the data are shown at the top of each panel for the weak line and at the bottom for the strong line. For Al III and Si IV, there is good agreement of the $N_a(v)$ profiles within each doublet, indicating that there is little unresolved saturated structure present within the lines. However, for C IV the weak line values of $N_a(v)$ significantly overestimate those for the strong line indicating that substantial saturation corrections are necessary at these velocities, even for the weak line (see text for details).

result of decreasing amounts of Al III at higher $|z|$. The former interpretation seems more likely since the velocity broadening of the Al III distribution is less affected by Galactic rotation that the higher ions toward HD 116852, presumably as a result of its smaller scale height ($\sim$800 pc compared to >1 kpc for the high ions; Sembach & Savage 1994) and therefore smaller abundance at large line-of-sight distances.

6.2. *Midplane Densities*

The most direct way to determine the midplane densities of the highly ionized species in the Galactic disk is to measure their column densities toward stars within the disk, like those in this study. Table 6 contains estimates of n_0(Si IV) and n_0(C IV) for the three disk stars and n_0(Al III) and an upper limit for n_0(N V) for HD 104705. The listed errors reflect measurement errors associated with the column densities presented in Table 5 and do not account for uncertainties in the distances listed in Table 2. The Galactic averages listed in the table are from Sembach & Savage (1992), who measured column densities toward a large number of stars and fitted a single exponential density distribution to the ensemble of column densities as a function of the stellar distances from the Galactic plane. An alternative method for determining midplane densities for ions toward individual stars located at large distances from the Galactic plane is to model the profiles with an assumed density distribution and Galactic rotation curve as was done for the HD 116852 values in the table (Sembach & Savage 1994). This kinematical approach has been exploited successfully for several sight lines where Galactic rotation effects broaden the high ion profiles substantially and allow one to relate velocity to distance (see for example, Savage, Massa, & Sembach 1990; Sembach, Savage, & Massa 1991).

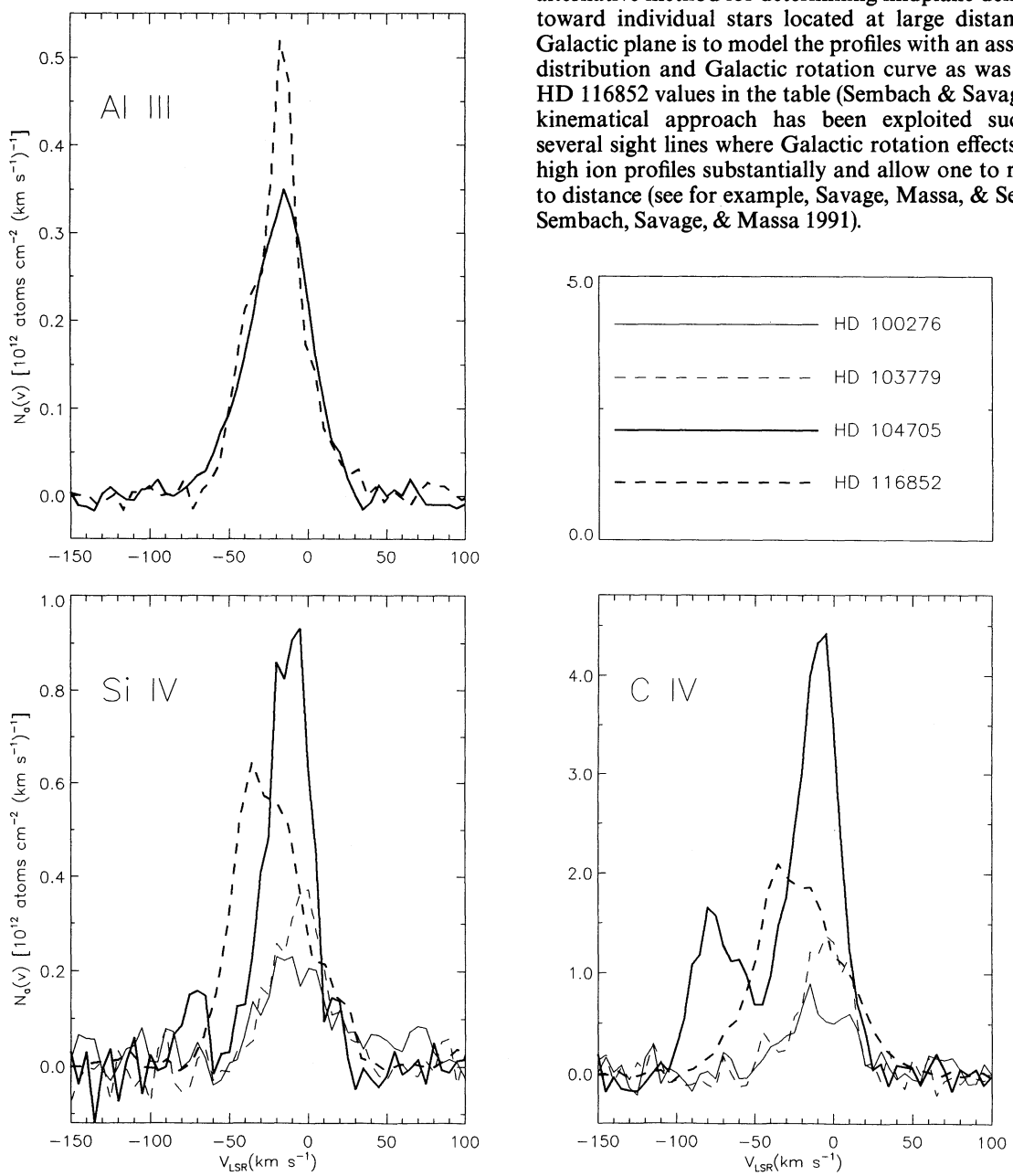

FIG. 7.—Comparison of the apparent column density profiles, $N_a(v)$ [atoms cm^{-2} (km s^{-1})$^{-1}$], as a function of LSR velocity for the Al III, Si IV, and C IV lines toward HD 100276, HD 103779, HD 104705, and HD 116852. For Al III and Si IV, the better determined strong line values of $N_a(v)$ are shown for each star. For C IV, the weaker λ1550 values of $N_a(v)$ are shown because saturation corrections are needed for the HD 104705 data. The HD 104705 C IV values are lower limits since unresolved saturated structure exists over the velocity range from -100 to $+20$ km s^{-1}. The HD 116852 data are from the GHRS study of this star by Sembach & Savage (1994) and have resolutions of 11, 16, and 14 km s^{-1} (FWHM) for Al III, Si IV, and C IV, respectively.

TABLE 4

APPARENT COLUMN DENSITIES

Ion	Line	$v_{LSR} = -130$ to -50 km s^{-1}			$v_{LSR} = -50$ to $+60$ km s^{-1}			$v_{LSR} = +60$ to $+110$ km s^{-1}		
		log N_a (-1σ)	log N_a	log N_a ($+1\sigma$)	log N_a (-1σ)	log N_a	log N_a ($+1\sigma$)	log N_a (-1σ)	log N_a	log N_a ($+1\sigma$)
					HD 100276					
Si IV	1402	...	...	12.34	12.90	13.10	13.15	12.11	12.41	12.58
	1393	...	12.20	12.46	13.04	13.10	13.16	11.98	12.19	12.33
C IV	1550	...	11.76	12.66	13.46	13.53	13.60	12.23	12.58	12.78
	1548	...	12.13	12.62	13.62	13.66	13.69	12.65	12.80	12.90
					HD 103779					
Si IV	1402	...	...	12.53	12.70	13.02	13.20	...	11.88	12.82
	1393	...	...	12.21	13.08	13.15	13.20	...	11.76	12.13
C IV	1550	...	...	12.62	13.68	13.73	13.78	...	...	12.29
	1548	...	...	12.50	13.78	13.82	13.85	...	11.99	12.44
					HD 104705					
Al III	1862	...	11.74	12.17	13.12	13.17	13.21	...	...	11.76
	1854	12.06	12.21	12.32	13.16	13.18	13.20	...	...	11.30
Si IV	1402	12.39	12.80	13.00	13.46	13.54	13.60	...	11.89	12.33
	1393	11.93	12.50	12.74	13.44	13.50	13.55	...	...	11.94
C IV	1550	13.71	13.75	13.79	14.18	14.20	14.23	...	11.56	12.40
	1548	13.45	13.52	13.57	13.98	14.04	14.08	...	11.58	12.36
N V	1238	...	...	12.61	...	12.23	12.77	...	...	...

The midplane densities for Si IV and C IV for HD 100276 and HD 103779 are very similar and are approximately a factor of 2 smaller than the Galactic averages. The HD 104705 Si IV midplane density is comparable to the Galactic average, but the C IV midplane density is a factor of 2 higher than the HD 116852 value and a factor of 3 higher than the Galactic average. The midplane density of Al III for the HD 104705 sight line is about a factor 2.5 less than that inferred for the HD 116852 or Galactic average sight lines.

6.3. *Column Density Ratios*

Column density ratios for the ionized species are presented in Table 6 for the HD 100276, HD 103779, HD 104705, and HD 116852 sight lines. These ratios are derived from the column densities and errors listed in Table 5. The similarity of the N(C IV)/N(Si IV) ratios along the HD 100276, HD 103779, and HD 116852 sight lines suggest that similar mechanisms are responsible for the creation of Si IV and C IV in these directions. Along these sight lines the ratio is close to the Galactic average of 3.6 ± 1.3, even though there appears to be about a factor of 2 less highly ionized gas in the disk toward HD 100276 and HD 103779 than toward HD 116852. Toward HD 104705, the C IV to Si IV ratio is considerably larger, N(C IV)/N(Si IV) ≈ 11. The larger HD 104705 ratio is directly attributable to the large amount of C IV along the sight line compared to the average amount of Si IV seen. The large amount of C IV along the HD 104705 sight line also appears to be the main reason for the large C IV to N V ratio along the sight line, N(C IV)/N(N V) > 10.

6.4. *The Highly Ionized Gas Fraction*

It is possible to place limits on the amount of silicon present as Si IV by comparing the column densities of adjacent ionization states. The most straightforward method of calculating column densities of Si II and Si III is to integrate apparent column density profiles for these species constructed from the absorption profiles illustrated in Figures 1–3. The column densities derived from the $N_a(v)$ profiles for the Si II λ1808 and Si III λ1206 lines are lower limits to the true column densities because the profiles contain unresolved saturated structures. Table 7 contains estimates of N(Si II) and N(Si III), as well as N(Si IV)/N(Si), for the HD 100276, HD 103779, and HD 104705 sight lines. The total amount of silicon present as Si IV along these sight lines is small ($< 2\%$). This Si IV ionization fraction is typical of highly ionized gas in the Milky Way and is very different from the large Si IV fractions found for QSO absorbers (York et al. 1991; C. Steidel 1994, private communication).

7. PRODUCTION OF THE HIGHLY IONIZED GAS

Sembach & Savage (1992) have summarized the status of various ionization mechanisms and models for the production of highly ionized gas in the Galactic halo. Below, I address some of these issues as they pertain to the Si IV, C IV, and N V observations for disk gas in the $l = 295°$, $b = 0°$ direction and direct the reader to the recent reviews by Spitzer (1990) and McKee (1993) for further details about other ionization stages and ionized gas topics in general.

7.1. *Photoionization versus Collisional Ionization*

One of the major obstacles in understanding the origin of the highly ionized gas traced by Si IV, C IV, and N V is determining to what extent the higher ionization stages are produced by photoionization in warm gas as opposed to collisional ionization in gas near 10^5 K. Photoionization is most impor-

TABLE 5

ADOPTED COLUMN DENSITIES[a]

Object	N(Al III)	N(Si IV)	N(C IV)	N(N V)
		-130 km s^{-1} to -50 km s^{-1}		
HD 100276	...	<12.62	<12.85	...
HD 103779	...	<12.51	<12.80	...
HD 104705	<12.38	$12.67^{+0.03}_{-0.03}$	$14.27 \pm {}^{+0.49}_{-0.49}$	<13.28
HD 116852[b]	$11.93^{+0.15}_{-0.23}$	$12.56^{+0.05}_{-0.06}$	$13.18^{+0.03}_{-0.03}$	<13.13
		-50 km s^{-1} to $+60$ km s^{-1}		
HD 100276	...	$13.07^{+0.09}_{-0.10}$	$13.60^{+0.05}_{-0.05}$	...
HD 103779	...	$13.09^{+0.12}_{-0.16}$	$13.78^{+0.04}_{-0.04}$	...
HD 104705	$13.17^{+0.03}_{-0.03}$	$13.52^{+0.06}_{-0.07}$	$14.45^{+0.17}_{-0.17}$	<13.36
HD 116852[b]	$13.23^{+0.03}_{-0.03}$	$13.64^{+0.02}_{-0.02}$	$14.10^{+0.02}_{-0.02}$	$13.41^{+0.04}_{-0.05}$
		$+60$ km s^{-1} to $+110$ km s^{-1}		
HD 100276	...	$12.31^{+0.36}_{-0.71}$	$12.70^{+0.14}_{-0.21}$	...
HD 103779	...	<12.18	<12.55	...
HD 104705	<12.06	<12.69	<12.78	...
HD 116852[b]	<11.97	<12.25	<11.98	<12.61

[a] Column densities and $\pm 1\ \sigma$ errors derived from the apparent column densities listed in Table 4 according to the prescription outlined in the text. All limits are 2 σ limits. All values agree with those obtained from a single component, Doppler-broadened curve of growth analysis.

[b] HD 116852 column densities derived from the Goddard High Resolution spectrograph observations presented by Sembach & Savage 1994.

tant for Si IV since only 33 eV is required for its creation, as opposed to 48 eV for C IV and 77 eV for N V. Previous considerations of this problem for Si IV have concluded that the majority of Si IV along halo sight lines must be produced by processes comparable to those producing C IV based upon the similarities in the line shapes of the two ions and the relatively constant N(C IV)/N(Si IV) ratio of 3.6 ± 1.3 found in the Galaxy (Sembach & Savage 1992). For a large fraction of the Si IV and C IV along extended sight lines through the disk and halo to be produced by photoionization by starlight rather than by collisional ionization requires ionization fields that are relatively constant over several kiloparsecs. This seems unlikely and for some sight lines can be ruled out completely. For example, very high resolution (FWHM ≈ 3.5 km s^{-1}) observations of the structured C IV and Si IV absorption toward HD 167756 ($l = 351°$, $b = -14°$, $d = 4$ kpc, $z = -0.85$ kpc; Savage et al. 1994) reveal several absorption complexes separated in velocity space, each with N(C IV)/N(Si IV) $\approx$ 3.5. It is equally difficult to explain why the integrated C IV to Si IV ratios along widely different directions within the Galaxy seem to be so

TABLE 6

SIGHT LINE COLUMN DENSITY RATIOS AND MIDPLANE DENSITIES[a,b]

				n_0(cm^{-3})				
SIGHT LINE	$\frac{N(\text{C IV})}{N(\text{Al III})}$	$\frac{N(\text{C IV})}{N(\text{Si IV})}$	$\frac{N(\text{C IV})}{N(\text{N V})}$	H I	Al III ($\times 10^9$)	Si IV ($\times 10^9$)	C IV ($\times 10^9$)	N V ($\times 10^9$)
HD 100276	...	3.0 ± 1.0	...	0.17	...	1.6 ± 0.5	4.7 ± 0.8	...
HD 103779	...	4.4 ± 1.4	...	0.11	...	1.0 ± 0.3	4.5 ± 0.7	...
HD 104705:								
-130 to -50 km s^{-1}	>79	~41:	>9.8	...	...	...	...	...
-50 to $+60$ km s^{-1}	19.1 ± 9.2	8.5 ± 4.3	>12.3	...	...	...	...	...
Total	26.9 ± 12.3	11.0 ± 5.2	>10.0	0.11	1.3 ± 0.1	3.2 ± 0.5	35 ± 13	<3.5
HD 116852[c]	7.4 ± 0.8	3.9 ± 0.2	4.5 ± 0.8	0.18	3.2 ± 0.2	3.5 ± 0.2	15 ± 1	3.7 ± 0.6
"Galactic Average"[d]	14.3 ± 6.6	3.6 ± 1.3	4.6 ± 2.7	0.15	3.1	4.1	11	5.1

[a] Column density ratios and $\pm 1\ \sigma$ errors are derived from the column densities listed in Table 5.

[b] Approximate midplane densities are derived from the column densities listed in Table 5 and the line of sight distances listed in Table 1. Errors account only for the column density errors listed in Table 5 and do not reflect distance uncertainties. All material is assumed to be distributed uniformly along the sight lines.

[c] HD 116852 values are from Sembach & Savage 1994. Average midplane densities are determined from kinematical models of the line profiles assuming that the gas density decreases exponentially as a function of distance from the plane.

[d] "Galactic Average" values are from Sembach & Savage 1992, except for n_0(H I) which is from Sembach & Danks 1994 and is the neutral hydrogen midplane density appropriate for the low-density H I component in the Galaxy. Average midplane densities are determined from an $N \mid \sin b \mid$ analysis of a single exponential density distribution fitted over many sight lines.

TABLE 7

Si IV IONIZATION FRACTION AND COLLISIONAL IONIZATION EQUILIBRIUM TEMPERATURES[a]

Object	N(Si II)[a]	N(Si III)[b]	N(Si IV)[c]	$\frac{N(\text{Si IV})}{N(\text{Si})}$	log T_{ed}[d]
HD 100276:					
-50 to -60 km s^{-1}	>15.43	...	13.07	$<4.3 \times 10^{-3}$	<4.45
HD 103779:					
-50 to -60 km s^{-1}	>15.29	...	13.09	$<6.3 \times 10^{-3}$	<4.45
HD 104705:					
-130 to -50 km s^{-1}	>14.27	>13.06	12.67	$<2.3 \times 10^{-2}$	<4.50
-50 to -60 km s^{-1}	>15.35	>13.32	12.52	$<1.4 \times 10^{-2}$	<4.50

[a] Column density lower limits for Si II obtained from direct integration of the Si II λ1808 profile for which unresolved saturated structure exists.

[b] Column density lower limits for Si III obtained from direct integration of the Si III λ1206 profile for which unresolved saturated structure exists. For data points at velocities where $I(v)_{\text{Si III}} < 0$, the data points were replaced by the $+1\,\sigma$ variations found for the fixed pattern and statistical noise fluctuations in the continuum.

[c] Si IV column densities from Table 5.

[d] Temperature limit satisfied by the Si IV ion fraction according to the collisional ionization calculations given by Sutherland & Dopita 1993. The alternate solutions at large temperatures, log $T > 5.10$, violate the low ion fractions.

similar if photoionization by starlight is a main contributor to the Si IV column.

Besides having difficulty producing substantial amounts of C IV, photoionization models predict large amounts of intermediate ionization stages such as Al III compared to Si IV and the higher ions. Sokolowski (1994) finds N(Al III)/N(Si IV) ≥ 50 for typical abundances in a dusty ISM and reasonable assumptions about the ionization field within the Galaxy due to hot stars, stellar remnants, and the X-ray background (see his Table 4). Combining these results with the observed abundances of Al III seen along the HD 104705 or HD 116852 sight lines leads to the conclusion that less than 1% of the observed Si IV arises from photoionization by the dilute Galactic radiation field. This result differs considerably from earlier estimates of the high ion abundances produced in a Galactic halo subject to a metagalactic radiation background as well as internal sources (Bregman & Harrington 1986; see also Fransson & Chevalier 1985). Ionizing radiation from extragalactic sources probably does not affect the ionization along disk sight lines appreciably unless the disk and halo are very porous to hard photons; attenuation by neutral gas effectively shields the underlying disk gas and sets up a vertical ionization structure in which there is little high ion gas in the Galactic disk, a result in conflict with the observations (Savage et al. 1990; Sembach, Savage, & Massa 1991). The same models also have difficulty reproducing both the observed column densities of the high ions and the ion fractions calculated in § 6.

A final piece of information to keep in mind when considering a photoionization versus collisional ionization origin for the highly ionized species is that localized sources of ionizing radiation may be important for some of the Si IV. Photoionization models of H II regions around young stars show that the amount of Si IV expected for thses types of stars is comparable to the observed amounts (Cowie, Taylor, & York 1981). However, the general similarities in the shapes of the Si IV and C IV profiles indicate that much of the observed Si IV is probably being formed with the C IV. The H II regions around these stars would produce less than about one-tenth of the observed C IV along the sight lines (see Cowie et al. 1981). Sembach, Savage, & Jenkins (1994) find N(Al III)/N(Si IV) ≈ 0.5 for the H II region surrounding ζ Oph, and O9.5 V star with a surface temperature somewhat hotter than those of the stars in this study. No detectable C IV absorption associated with the ζ Oph H II region was found. The ζ Oph N(Al III)/N(Si V) ratio is similar to the integrated ratios found for the HD 104705 and HD 116852 sight lines in this study. A photoionization origin in line-of-sight H II regions for some of the ionized species, particularly Al III and Si IV, cannot be ruled out completely based upon ionic ratios alone, but seems somewhat unlikely given that the cross-sectional areas of the Si IV–bearing regions are small (see Cowie et al. 1981). A second, and perhaps more important, localized source of ionizing photons is from recombinations in cooling hot gas (Slavin & Cox 1992; Sembach & Savage 1992; Shapiro & Benjamin 1993), as discussed in following sections.

7.2. *Collisional Ionization Equilibrium*

The widths of the high ion lines toward HD 100276, HD 103779, and HD 104705 place only loose constraints on the temperature of the gas, $T < 5 \times 10^5$ K, because the lines are broadened by a combination of Galactic rotation (as much as 30 km s^{-1}; see Table 2), cloud-to-cloud motions, and intrinsic nonthermal broadening within individual parcels of the highly ionized gas. In collisional ionization equilibrium the Si IV ion fractions listed in Table 7 imply that the gas must have log $T < 4.5$ and an equivalent H^+ column density of $\sim 3.1 \times 10^{19}$ cm^{-2}, which is about 2.5% of the H I column along the sight lines assuming the solar abundances given by Anders & Grevesse (1989). If the Si IV arises in collisionally ionized gas below log $T \approx 4.5$, the associated amount of hydrogen in the form of H^+ increases rapidly.

The similarity of the Si IV and Al III profiles along the HD 104705 (and HD 116852) sight line at some velocities suggests that portions of the absorbing medium traced by the two ions may be related. Al III is abundant in collisionally ionized gas at temperatures between about 2×10^5 K and 5×10^5 K

(Hartquist, Snijders, & West 1983) and should exist only in regions where Si III is abundant [$\chi_{II,II}$(Al) = 18.8, 28.8 eV; $\chi_{II,II}$(Si) = 16.3, 33.5 eV; Moore 1970]. Hartquist et al. (1983) argue that Al III should not be abundant in gas that is cooling rapidly from large temperatures ($T > 5 \times 10^4$ K) and should not coexist with Si IV and C IV. Si III produced by fast shocks should also exist at temperatures below about 8×10^4 K (Shull 1977), and the HD 104705 N(Si III)/N(Al III) ratios of >4.8 for the -130 to -50 km s^{-1} absorption and >1.4 for the -50 to $+60$ km s^{-1} absorption are consistent with the Al III and Si III tracing the same gas.

In the preceding discussion, the collisional ionization equilibrium arguments are based upon the assumption that the different ionization stages are well mixed. Coincidences in velocity structure between neutral and ionized species can also occur for species within clouds and their boundary layers. Nonequilibrium effects are very important for Si IV and C IV since gas near the peak of the cooling curves for these ions cools faster than it recombines (Shapiro & Moore 1976; Sutherland & Dopita 1993), and therefore the predicted ionization fractions for Si IV and C IV at low temperatures may be larger than those expected in equilibrium situations. For this reason, I now consider models accounting for the time-dependent, nonequilibrium cooling of hot gas in the presence of cooler material.

7.3. *Turbulent Mixing Layers*

Many collisional ionization models fare no better than photoionization models in reproducing the observed high ion column density ratios. However, one that is relatively successful is the turbulent mixing layer (TML) model of Slavin, Shull, & Begelman (1993; see also Begelman & Fabian 1990) in which hot ($T \sim 10^6$ K) and warm ($T \sim 10^4$ K) gas mix together in the presence of turbulent motions within shear flows at the boundaries of the gas layers.

Turbulent mixing layers can reproduce the observed values of N(C IV)/N(Si IV) $\approx$ 3–4 along the HD 100276 and HD 103779 sight lines (see Table 6) provided that the temperature of the postmixed gas, $\bar{T}$, is about 2×10^5 K and the entrainment velocity of the hot gas, v_t, is between 25 and 100 km s^{-1}. A useful constraint on the entrainment velocity can be set by comparing the column densities predicted per TML with the observed frequency of low ionization absorption sites. For $\bar{T} \approx 2 \times 10^5$ K, $v_t \approx 25$ km s^{-1} yields log N(C IV) per TML = 11.20, which leads to at least 75 TMLs per kiloparsec, a requirement in severe disagreement with the observed number of neutral clouds observed along these sight lines (Figs. 1 and 2; § 6). For $\bar{T} \approx 2 \times 10^5$ K, $v_t \approx 100$ km s^{-1} yields log N(C IV) per TML $\approx$ 12.30. This requires approximately six neutral clouds per kiloparsec and is consistent with the Na I and Ca II observations if there are unresolved components present. The typical interstellar neutral cloud frequency is about five clouds per kiloparsec (Hobbs 1974).

The TML models also appear to be able to reproduce both the large N(C IV)/N(Si IV) $\approx$ 8.5 and N(C IV)/N(N V) $\geq$ 12 ratios toward HD 104705 in the -50 to $+60$ km s^{-1} absorption complex. A temperature near $\bar{T} \approx 2 \times 10^5$ is required to satisfy the observed ratios, although the C IV to Si IV ratio is underestimated by about a factor of two for the $v_t = 100$ km s^{-1} case. From the general trends present in TML column densities listed by Slavin et al. as a function of both v_t and $\bar{T}$, it is possible that increasing the entrainment velocity of the hot gas to a value in excess of 100 km s^{-1} for the $\bar{T} \approx 2 \times 10^5$ case would lead to ionic ratios compatible with the observations. A slight temperature increase may also be appropriate, although even 50% changes in $\bar{T}$ at these temperatures increases the N(C IV)/N(Si IV) ratio by approximately an order of magnitude. Mixing layer models with $\bar{T} \approx 3 \times 10^5$ and $v_t \approx 100$ km s^{-1} satisfy both the N(C IV)/N(N V) > 10 and N(C IV)/N(Si IV) $\sim$ 40 ratios for the -130 to -50 km s^{-1} complex.

Note that the large values of v_t inferred above for the three sight lines on the basis of column density ratios are not observationally excluded by the observed line widths. The physical velocity found in a turbulent layer depends upon both v_t and on the hot gas mass fraction in the flow, η_h. The observed widths indicate that $\eta_h \leq 0.5$–0.7 if $v_t \approx 100$ km s^{-1}.

The success of the TML models in accommodating a wide variety of high ion column density ratios with only slight variations in the mixing layer parameters may also be their biggest drawback; slight changes in the TML parameters lead to large changes in the model predictions, thereby making it difficult to distinguish among models spanning a large fraction of observationally relevant parameter space. If mixing layers are responsible for both the high ionization lines seen toward HD 104705 in this study and those seen toward the poles by Savage & Sembach (1994), then the entrainment velocity or the fraction of mass deposited by the hot gas in the turbulent flow may be higher in the disk than in the halo.

7.4. *Conduction Fronts*

A class of models that meets with limited success in reproducing the observed high ion column densities and ratios is one that examines the thermal conduction fronts between warm and hot media in the presence of a magnetic field (Borkowski, Balbus & Fristrom 1990). Savage et al. (1994) favor conduction fronts in late evaporative or early condensing stages, $t > 10^6$ yr, to explain the constancy of the N(C IV)/N(Si IV) = 3.5 ratio found for several gas parcels toward HD 167756. Although the models overestimate the observed C IV to Si IV ratio by several times at this point in the front evolution, at these late stages recombination radiation from He II λ304 and similar lines may boost the Si IV abundance. The alternate solution for the N(C IV)/N(Si IV) $\approx$ 3–4 ratios like those seen toward HD 100276, HD 103779, and HD 116852 is that the fronts are very young, with $t \sim 10^3$ yr. For HD 104705, the fronts must have ages less than 10^4 yr when N(N V) < N(Si IV). However, these early stage solutions fail the ratio constancy criteria that probably exist for the HD 100276 and HD 103779 sight lines, and they also imply mean ionic temperatures of $T \sim 4 \times 10^5$ K. In the most opportune situation, the $\sim$45 km s^{-1} widths (FWHM) of the C IV lines toward the stars could be due to a single thermally broadened component having a gas temperature near $(4.5$–$5) \times 10^5$ K. However, the profile widths must have contributions from overlapping absorption components along the sight line, macroscopic internal cloud motions, and Galactic rotation broadening. Therefore, it is impossible to reconcile the observed widths with fronts in early stages of evolution.

For HD 104705, the conduction front models cannot account for the large N(C IV)/N(N V) ratio and the observed profile widths. For these species, the seriousness of the discrepancy between observation and theory is much more severe than it is for Si IV because recombination radiation within the cooling hot gas is not important and aggravates the situation if it contributes to the C IV column density.

7.5. *Supernova Remnants*

Slavin & Cox (1992) have calculated column densities for an average sight line through a supernova remnant as a function of time. They find N(C IV)/N(Si IV) $\approx$ 12–23 and N(C IV)/N(N V) $\approx$ 1.9–2.3. The bubbles cool mainly by line radiation in a thick shell of compressed material, and it is therefore unlikely that different viewing geometries affect these ratios significantly. Taken at face value, these models fail to match the observed N(C IV)/N(Si IV) ratio along the HD 100276, HD 103779, and HD 116852 sight lines and the observed N(C IV)/N(N V) ratio along the HD 104705 sight line. The former discrepancy could potentially be removed by the incorporation of recombination line radiation as in the conduction front models, but the latter discrepancy requires alternate solutions.

One possible explanation for the large N(C IV)/N(N V) ratio toward HD 104705 might be that the initial heating of the gas is never sufficient to produce appreciable amounts of N V and higher ionization stages but is still high enough to produce Si IV and C IV. Regardless of the hot gas model employed, this may be the best solution for the large C IV to N V ratio, and it leads to the interesting possibility that larger C IV to Si IV ratios do not necessarily imply that the gas is more highly ionized; in fact, the reverse may be true. This effect is evident in the TML calculations presented by Slavin et al. (1993; see their Table 3).

Typical supernova bubbles should have N(C IV) $\approx 10^{13}$ cm^{-2} according to the Slavin & Cox calculations, and therefore one expects approximately 1.5 bubbles per kpc for the HD 100276 and HD 103779 sight lines and 10 bubbles per kpc for the HD 104705 sight line. The HD 100276 and HD 103779 values are slightly less than the value of two to three bubbles per kpc required for the halo gas observations made by Sembach & Savage (1992) and are comparable to the number of O VI–bearing bubbles found by Shelton & Cox (1993; see also Slavin & Cox 1993) based upon a reanalysis of the O VI data presented by Jenkins (1978a, b). The large number of bubbles required for the HD 104705 sight line may be yet another indicator that SNRs are not be dominant source of the absorption along the sight line.

7.6. *Cooling Flows*

The standard high ion column density ratios found in the Galaxy along sight lines like HD 100276 and HD 103779 can be partially explained in terms of large-scale cooling flows. Self-ionization within plane parallel flows is paramount in creating enough Si IV to match the observations and produce N(C IV)/N(Si IV) ratios near 3.5 (Shapiro & Benjamin 1991). The importance of self-ionization within the isochorically cooling flows stands in contrast to the finding by Slavin et al. (1993; J. D. Slavin 1994, private communication) that the effects of self-ionization within the isobarically cooling hot gas of turbulent mixing layers are negligible. However, the details of the self-ionization calculations in the two models may differ. Properly incorporating the radiative transfer required to account for the self-ionizing radiation in the cooling flows appears to be just as important as the presence of the radiation itself; it reduces the size of the cooling regions from $D > 1$ kpc to $D \sim 40$ pc (Shapiro & Benjamin 1993), which is in general agreement with the 50–100 pc sizes for the high-ion regions found in this study.

Whether the cooling flow models can reproduce the nonstandard high-ion column density ratios toward HD 104705 remains to be determined. The variability of the high-ion ratios on the small angular scales found in this study places severe limitations on the conclusions that can be drawn from models that attempt to reconcile the high-ion absorption-line data with C IV and O III emission line measurements obtained for only a few sight lines.

8. HIGH-ION ABSORPTION AND THE CIRCUMSTELLAR ENVIRONMENT

Some of the high-ion absorption detected toward HD 100276, HD 103779, and HD 104705 may arise in the circumstellar environments of the stars as the stellar winds interact with the ambient interstellar medium. The amount of mass swept up in an interstellar bubble depends upon the stellar wind and local ISM properties (see eqs. [4]–[8] of Castor, McCray, & Weaver 1975). Observational information on wind bubbles around other stars is limited, although a recent study of the ζ Oph sight line (Sembach et al. 1994) finds log N(C IV) $\approx$ 12.73 and log N(Si IV) $\approx$ 11.82 for the wind/ISM interface. Sembach & Savage (1994) find a similar C IV column density limit, log N(C IV) $<$ 12.94, for the HD 116852 sight line, even though the wind speed is much higher [v_∞(C IV) $\approx$ 2600 km s^{-1}]. The high-ion column densities for circumstellar bubbles around the stars in this study should be less than for the ζ Oph sight line since the stellar wind speeds are comparable [v_∞(C IV) = 1640, 1660, and 1740 km s^{-1} for HD 100276, HD 103779, and HD 104705 compared v_∞(C IV) = 1400 km s^{-1} for ζ Oph] and the ambient interstellar medium densities are probably smaller ($n \approx$ 4–10 cm^{-3} for ζ Oph). If one adopts a value of N(C IV) = 10^{13} cm^{-2} as being typical (see §§ 7.4 and 7.5), less than about 20% of the HD 100276 and HD 103779 C IV columns and less than 3% of the HD 104705 column can arise in such an interface. Note that this also argues strongly against a single interface origin for the -130 to -50 km s^{-1} C IV absorption toward HD 104705.

9. THE DISK-HALO CONNECTION

One of the fundamental issues to be addressed in studies of highly ionized gas in the Galaxy is the relationship, or lack thereof, of hot gas in the disk to gas in the halo. Almost all models of the production and support of highly ionized gas at large z-distances require the existence of regions of highly ionized gas in the disk as well, either at the locations where the gas escapes into, or returns from, the Galactic halo. Possible mechanisms for driving gas out of the disk and into the halo include Galactic fountains (Shapiro & Field 1976; Chevalier & Oegerle 1979; Bregman 1980; Houck & Bregman 1990; Li & Ikeuchi 1992; Shapiro & Benjamin 1991, 1993) and stellar winds and star formation (Rosen, Bregman, & Norman 1993). The Galactic fountain models can also qualitatively explain the motions of neutral high-velocity clouds in the halo (Shapiro & Field 1976; Houck & Bregman 1990; Li & Ikeuchi 1992).

The ability of superbubbles or hot gas chimneys produced by supernovae to break out of the gas layer of the disk (see Mac Low, MacCray, & Norman 1989; Norman & Ikeuchi 1989) depends upon the particle density and orientation of the magnetic field within the gas. Magnetic fields have a confining influence on supernovae (Cui & Cox 1992; Slavin & Cox 1992; Edgar & Cox 1993). It may be easier for gas to move parallel to the disk than away from the disk if either the density gradient in the horizontal direction is less than in the vertical direction

or if the magnetic field orientation is favorably aligned (see Mineshige et al. 1993). The former possibility seems unlikely, but Bloemen (1987) has shown that large-scale horizontal magnetic field orientations can be stable and have a confining influence on the hot gas content of the Milky Way in the vertical direction. Interarm regions are likely areas for superbubbles to break into if they cannot vent directly into the halo because the magnetic field strengths in interarm regions should be less than in spiral arms due to the lower gas densities. Supernovae occurring near the edges of spiral arms could vent their energy into interarm regions before the hot gas escapes into the halo and thereby establish a "kinked" Galactic fountain.

Observational signatures of such a kinked fountain might include increased ionization levels and larger velocities in disk gas compared to halo gas. Recent theoretical work concerning the production of highly ionized gas in the Milky Way suggests that there may be multiple phases of the hot gas and that the relative proportions of the highly ionized species should change as a function of distance from the Galactic plane (Shull & Slavin 1994). The similarity of the N(C IV)/N(Si IV) ratio toward HD 100276, HD 103779, and HD 116852 favors similar conditions for the disk and low halo gas, and the high ion absorption velocities on the positive velocity portion of the profiles, where there should be no direct Galactic rotation influences, are comparable. However, the presence of a distinct absorption complex centered near -75 km s^{-1} toward HD 104705 argues that at least some of the gas must be moving at velocities of 40 km s^{-1} or more in excess of those predicted for the sight line or seen in the neighboring disk lines. This negative velocity gas may give rise to some of the higher z gas seen toward HD 115852 at comparable velocities. Also, as discussed above the turbulent mixing layer models, the gas toward HD 104705 may have larger hot gas entrainment velocities than pure halo sight lines.

10. CONCLUSIONS

The main results of this study of highly ionized gas in the $l = 295°$, $b = 0°$ interarm disk directions are as follows:

1. Comparisons of the Si IV and C IV absorption along the extended disk sight lines toward HD 100276, HD 103779, and HD 104705 reveal that the high ion absorption shows large variations on scales of 50–100 pc.

2. Comparisons of the HD 104705 and HD 116852 sight lines reveal that the highly ionized gas created in the Galactic disk may differ appreciably from that along low halo sight lines in similar directions. Further investigations of highly ionized gas along other sight lines are required to determine if this is a common occurrence or if the $l = 295°$ direction is unique in this respect.

3. The high ion ionization fraction is less than about 2% along these sight lines. The amount of H^+ associated with the highly ionized gas is small, less than 2% of the H I, unless the high ionization species occur in gas with temperatures below 3×10^4 K.

4. The Si IV and C IV midplane densities derived for HD 100276 and HD 103779 are factors of 2 lower than the Galactic averages, n_0(Si IV) $= 4.1 \times 10^{-9}$ cm^{-3} and n_0(C IV) $= 1.1 \times 10^{-8}$ cm^{-3}, whereas the Si IV midplane density toward HD 104705 is near the average value, and the C IV midplane density is a factor of 3 higher than average.

5. The integrated C IV to Si IV ratios along the HD 100276 and HD 100379 sight lines are similar to the N(C IV)/N(Si IV) $= 3.6 \pm 1.3$ ratio found by Sembach & Savage (1992) for a sample of halo stars. For the HD 104705 sight line, N(C IV)/N(Si IV) $= 11$ and N(C IV)/N(N V) > 10. The large values of these ratios are due to the very large quantity of C IV along this sight line.

6. Turbulent mixing layers are possible sites for the production of highly ionized gas in the Galactic disk. The mixing layer models require large entrainment velocities, $v_t \geq 100$ km s^{-1}, and postmixed gas temperatures, $\bar{T} \geq 2 \times 10^5$ K. If mixing layers are responsible for the observed absorption toward HD 104705 and in the halo toward the Galactic poles (Savage & Sembach 1994), then either the entrainment velocity or the fraction of mass deposited by the hot gas in the turbulent flow may be higher in the disk than in the halo.

7. The observed high ion column density ratios cannot be reproduced by time-averaged values of these quantities in models of evolving supernova remnants or conduction fronts.

8. While cooling flow models are able to reproduce the observed small N(C IV)/N(Si IV) ratios along the HD 100276, HD 103779, and HD 116852 sight lines, it is uncertain whether they can also reproduce the large N(C IV)/N(Si IV) and N(C IV)/N(Si IV) ratios along the HD 104705 sight line. Altering the initial temperature of the heated gas may be able to account for the HD 104705 ratios.

9. More work clearly needs to be done on both the theoretical and observational fronts to understand better the processes giving rise to the ubiquitous N(C IV)/N(Si IV) ratio and the possible circumstances under which it may depart drastically from its average value of 3.6 ± 1.3, as it does for the HD 104705 sight line.

I thank the dedicated people of the *IUE* project for scheduling and implementing the remote observations required for this study. All remote observations, data reduction, and analysis for this study were performed at the Massachusetts Institute of Technology. It is a pleasure to thank Robert Benjamin and Blair Savage for interesting discussions concerning highly ionized gas in the Galaxy, and I also appreciate the helpful comments of the referee. I gratefully acknowledge support from a Hubble Fellowship provided by NASA through grant HF-1038.01-93A from the Space Telescope Science Institute, which is operated by AURA under NASA contract NAS 5-26555.

REFERENCES

Anders, E., & Grevesse, N. 1989, Geochim. Cosmochim. Acta, 53, 197
Begelman, M. C., & Fabian, A. C. 1990, MNRAS, 244, 261
Bloemen, J. B. G. M. 1987, ApJ, 322, 694
Bok, B. J. 1971, Highlights Astr., 2, 63
Borkowski, K. J., Balbus, S. A., & Fristrom, C. C. 1990, ApJ, 355, 501
Bregman, J. N. 1980, ApJ, 236, 577
Bregman, J. N., & Harrington, P. J. 1986, ApJ, 309, 833
Castor, J., McCray, R., & Weaver, R. 1975, ApJ, 200, L107
Chevalier, R. A., & Oegerle, W. R. 1979, ApJ, 277, 398
Courtès, G., Georgelin, Y. P., Georgelin, Y. M., & Monet, G. 1970, in IAU Symp. 38, The Spiral Structure of Our Galaxy, ed. W. Becker & G. Contopoulos (Dordrecht: Reidel), 209
Cowie, L. L., Taylor, W., & York, D. G. 1981, ApJ, 248, 528
Cui, W., & Cox, D. P. 1992, ApJ, 401, 206
Diplas, A., & Savage, B. D. 1993, ApJ, 427, 274
Edgar, R. J., & Chevalier, R. A. 1986, ApJ, 310, L27
Edgar, R. J., & Cox, D. P. 1993, ApJ, 413, 190
Fransson, C., & Chevalier, R. A. 1985, ApJ, 296, 35

Heiles, C. 1982, ApJ, 262, 135
Hartquist, T. W., Snijders, M. A. J., & West, K. A. 1983, MNRAS, 203, 1183
Hobbs, L. M. 1974, ApJ, 191, 395
Houck, J., & Bregman, J. N. 1990, ApJ, 352, 506
Howrth, I. D., et al. 1993, ApJ, 417, 338
Jenkins, E. B. 1978a, ApJ, 219, 845
———. 1978b, ApJ, 220, 107
Johnson, H. L. 1963, in Stars and Stellar Systems, 3, Basic Astronomical Data, ed. K. A. Strand (Chicago: Univ. of Chicago Press), 214
Kerr, F. J., Bowers, P. F., Jackson, P. D., & Kerr, M. 1986, A&AS, 66, 373
Koo, B. C., Heiles, C., & Reach, W. T. 1992, ApJ, 390, 108
Li, F., & Ikeuchi, S. 1992, ApJ, 390, 405
Lu, L., Savage, B. D., & Sembach, K. R. 1994, ApJ, 436, 563
Mac Low, M.-M., McCray, R., & Norman, M. L. 1989, ApJ, 337, 141
McCammon, D., Burrows, D. N., Sanders, W. T., & Kraushaar, W. L. 1983, ApJ, 269, 107
McKee, C. 1993, in Back to the Galaxy, ed. S. Holt & F. Verter (New York: AIP), 499
Mihalas, D., & Binney, J. 1981, Galactic Astronomy (2d ed.; San Francisco: Freeman)
Mineshige, S., Shibata, K., & Shapiro, P. R. 1993, ApJ, 409, 663
Moore, C. E. 1970, Ionization Potentials and Ionization Limits Derived from the Analysis of Optical Spectra (Report NSRDS-NBS 34) (Washington: US Department of Commerce)
Morton, D. C. 1991, ApJS, 77, 119
Norman, C., & Ikeuchi, S. 1989, ApJ, 345, 372
Pettini, M., & West, K. A. 1982, ApJ, 260, 561
Prinja, R. K., & Howarth, I. D. 1986, ApJS, 61, 357
Prinja, R. K., Howarth, I. D., & Henrichs, H. F. 1987, ApJ, 317, 389
Rickard, J. J. 1974, A&A, 31, 47
Rosen, A., Bregman, J. N., & Norman, M. L. 1993, ApJ, 413, 137
Savage, B. D., et al. 1993a, ApJ, 413, 116
Savage, B. D., Lu, L., Weymann, R., Morris, S., & Gilliland, R. 1993b, ApJ, 404, 124
Savage, B. D., & Massa, D. 1987, ApJ, 314, 381
Savage, B. D., Massa, D., & Sembach, K. R. 1990, ApJ, 335, 114
Savage, B. D., & Sembach, K. R. 1991, ApJ, 379, 245
———. 1994, ApJ, 434, 145
Savage, B. D., Sembach, K. R., & Cardelli, J. 1994, ApJ, 420, 183
Sembach, K. R., & Danks, A. C. 1994, A&A, in press
Sembach, K. R., Danks, A. C., & Savage, B. D. 1993, A&AS, 100, 107
Sembach, K. R., & Savage, B. D. 1992, ApJS, 83, 147
———. 1994, ApJ, 431, 201
Sembach, K. R., Savage, B. D., & Jenkins, E. B. 1994, ApJ, 421, 585
Sembach, K. R., Savage, B. D., & Massa, D. 1991, ApJ, 372, 81
Shapiro, P. R., & Benjamin, R. A. 1991, PASP, 103, 923
———. 1993, in Star Forming Galaxies and Their Interstellar Media, ed. J. J. Franco (New York: Cambridge Univ. Press), 273
Shapiro, P. R., & Field, G. B. 1976, ApJ, 205, 762
Shapiro, P. R., & Moore, R. T. 1976, ApJ, 207, 406
Shelton, R., & Cox, D. 1993, in preparation
Shull, J. M. 1977, ApJ, 216, 414
Shull, J. M., & Slavin, J. D. 1994, ApJ, 427, 784
Slavin, J. D., & Cox, D. 1992, ApJ, 392, 131
———. 1993, ApJ, 417, 187
Slavin, J. D., Shull, J. M., & Begelman, M. C. 1993, ApJ, 407, 83
Snow, T. P. 1977, ApJ, 217, 760
Sokolowski, J. 1994, ApJ, submitted
Spitzer, L. 1990, ARA&A, 28, 71
Spitzer, L., & Fitzpatrick, E. 1992, ApJ, 391, L41
Sutherland, R. S., & Dopita, M. A. 1993, APJS, 88, 253
Walborn, N. R. 1972, AJ, 77, 312
York, D. G., Yanny, B., Crotts, A., Carilli, C., Garrison, E., & Matheson, L. 1991, MNRAS, 250, 24